Engineering Vertically Aligned Carbon Nanotube Growth by Decoupled Thermal Treatment of Precursor and Catalyst

Eric R. Meshot,[†] Desirée L. Plata,[‡,§] Sameh Tawfick,[†] Yongyi Zhang,[†] Eric A. Verploegen,[∥] and A. John Hart[†,*]

[†]Department of Mechanical Engineering, University of Michigan, 2350 Hayward Street, Ann Arbor, Michigan 48109, [‡]Department of Civil and Environmental Engineering, Massachusetts Institute of Technology, 15 Vassar Street, Cambridge, Massachusetts 02139, [§]Marine Chemistry and Geochemistry Department, Woods Hole Oceanographic Institution, Woods Hole, Massachusetts 02543, and [∥]Department of Materials Science and Engineering, Massachusetts Institute of Technology, 77 Massachusetts Avenue, Cambridge, Massachusetts 02139

ABSTRACT We study synthesis of vertically aligned carbon nanotube (CNT) "forests" by a decoupled method that facilitates control of the mean diameter and structural quality of the CNTs and enables tuning of the kinetics for efficient growth to forest heights of several millimeters. The growth substrate temperature (T_s) primarily determines the CNT diameter, whereas independent and rapid thermal treatment (T_p) of the C_2H_4/H_2 reactant mixture significantly changes the growth rate and terminal forest height but does not change the CNT diameter. Synchrotron X-ray scattering is utilized for precise, nondestructive measurement of CNT diameter in large numbers of samples. CNT structural quality monotonically increases with T_s yet decreases with T_p, and forests grown by this decoupled method have significantly higher quality than those grown using a conventional single-zone tube furnace. Chemical analysis reveals that the thermal treatment generates a broad population of hydrocarbon species, and a nonmonotonic relationship between catalyst lifetime and T_p suggests that certain carbon species either enhance or inhibit CNT growth. However, the forest height kinetics, as measured in real-time during growth, are self-similar, thereby indicating that a common mechanism of growth termination may be present over a wide range of process conditions.

KEYWORDS: carbon nanotube · aligned · kinetics · catalyst · X-ray scattering · chemical vapor deposition

Synthesis of carbon nanotubes (CNTs) by chemical vapor deposition (CVD) involves decomposition of carbon-containing molecules and the consequent self-assembly of graphitic carbon at nanoparticle growth sites.[1] The distinctive organization of an aligned "forest" of CNTs is further governed by physical interactions among large numbers of CNTs growing at microscopically fantastic speeds.[2] Manufacturing an infinite cable of continuous CNTs would possibly realize dreams of CNT-based cables and wires having stiffness, strength, and transport properties exceeding today's best metal alloys and advanced fibers. More immediately, precisely tuning the structural characteristics (*e.g.*, diameter, areal density) and quality of CNT forests, while establishing efficient reaction processes, is vital for commercial development of CNT-based electrical, thermal, and mechanical interface layers, as well as filtration membranes.[3−9] Despite extensive study of single-wall CNT (SWNT) and multi-wall CNT (MWNT) forest production,[2,10−24] including recent advances using water and oxygen as additives to increase reaction yield and catalyst lifetime, the limiting mechanisms of forest growth are not fully understood, and CNT forest heights are typically limited to several millimeters.

The process of CNT film growth by CVD typically involves multiple stages: (1) the catalyst is prepared on a substrate, such as a silicon wafer; (2) the catalyst is heated and treated chemically, such as by exposure to a reducing atmosphere that causes a thin film to agglomerate into nanoparticles; (3) the catalyst is exposed to a carbon-containing atmosphere, which causes formation and "liftoff" of CNTs from the nanoparticles on the substrate; and (4) CNT growth continues by competing pathways between accumulation of "good" (graphitic) and "bad" (amorphous) carbon.[25] To engineer the functional properties of CNT materials such as forests, we must develop reaction processes that not only treat these stages independently, but are also accompanied by characterization techniques that enable mapping of the forest characteristics for large sample sizes and populations.

*Address correspondence to ajohnh@umich.edu.

Received for review January 22, 2009 and accepted July 27, 2009.

Published online August 19, 2009.
10.1021/nn900446a CCC: $40.75

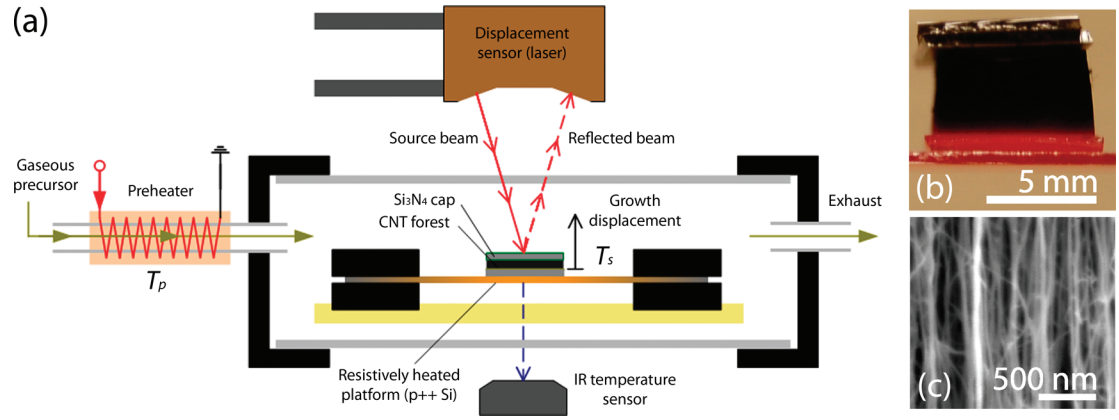

Figure 1. (a) Schematic representation of decoupled CVD apparatus where the reactant gases enter the reaction chamber after passing through a heated pipe maintained at T_p. The heated mixture deposits at the growth substrate, maintained at T_s. CNT forest height is measured in real time by a laser displacement sensor. (b) Digital photograph shows a CNT forest growing on the heated Si platform, while (c) shows the forest comprises well-aligned CNTs (T_s/T_p = 825/1020 °C).

We present a decoupled CVD method that enables precise tuning of CNT diameter, structural quality, and growth kinetics of vertically aligned CNT forests. While our study is restricted to a single catalyst composition and thickness, it demonstrates the importance of each process stage in determining the structural character of a CNT forest and the practical versatility that can be achieved by treating these process variables independently. Other methods of tuning CNT diameter include using porous templates such as anodic alumina,[26,27] as well as changing the particle size by building metal nanoparticles within micelles defined by block copolymers,[28−31] by high-resolution lithography,[32] or by changing the starting thickness of the catalyst thin film.[33,34] However, these approaches can be complicated and costly in mass production. The critical role of thermal decomposition of the reactant is typically manipulated by changing the reactant composition and flow rate[35−38] or by plasma-enhanced methods[35,39] and, to our knowledge, has not been addressed systematically as in the present study.

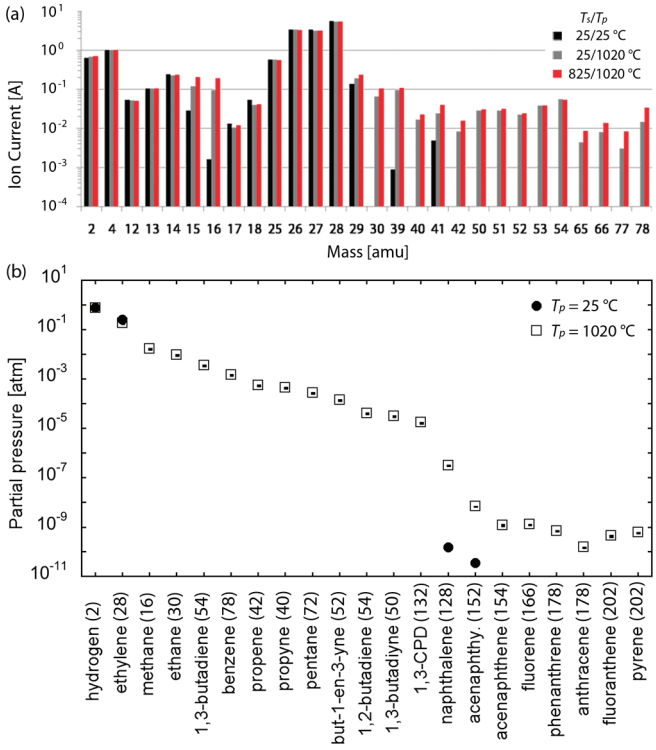

Figure 2. (a) Mass spectra collected *in situ* by a quadrupole mass spectrometer (MS) residual gas analyzer, demonstrating relative changes in the abundance of select compounds. Data is for thermal treatment of C_2H_4/H_2 = 0.2/0.5 atm. The ion current is normalized to mass 4 (attributed to He). (b) Using the same CVD system, our group (Plata, *et al.* [45]) showed that a thermally treated gas mixture of C_2H_4/H_2 = 0.2/0.8 atm, analyzed *ex situ* by GC−MS and GC−FID, contains a broad range of compounds whose abundances vary by several orders of magnitude. The nominal molecular weight of each species (in amu) is displayed with the name on the bottom axis, and the error bars represent one standard deviation on triplicate analyses of the same sample. 1,3-CPD = 1,3 cyclopentadiene; acenaphthy = acenaphthylene.

CNT forest growth is performed using a custom-built atmospheric pressure CVD reactor (SabreTube, Absolute Nano) shown in Figure 1a, wherein the growth substrate rests on a resistively heated silicon platform, which is maintained at temperature T_s.[40] Due to its low thermal mass, the substrate heats at approximately 200 °C s^{-1} when maximum power is applied. The forest height is measured in real time using a laser displacement sensor (Keyence LKG152) mounted above the chamber. The gas mixture enters the chamber through a heated quartz pipe (4 mm i.d.) that is maintained at temperature T_p. The residence time of the reactant mixture in the heated pipe is less than 0.1 s, and the gas cools to ambient (room) temperature before entering the reaction chamber and reaching the growth substrate, where the quartz tube wall does not exceed 70 °C (as measured by surface-mounted thermocouples).

Using this decoupled system, the gas can be "preheated" to temperatures much higher than those used in a typical single-zone tube furnace CNT growth process, wherein the gas treatment and catalyst treatment temperatures are coupled. If a tube furnace were used, the much longer residence time at such high tempera-

tures would cause excessive gas-phase decomposition and rearrangement of the reactant, leading to contamination of the growth environment. We previously demonstrated that thermal decomposition of C_2H_4 is necessary for rapid growth of tall CNT forests in this decoupled system.[41] This contrasts "hot filament" methods wherein a wire heated to over 1500 °C is placed near the substrate.[42−44] In our approach, direct flow through a heated pipe ensures uniform activation of the gas; a short residence time ensures that significant sooting is avoided, and the activation temperature of the gas is fully decoupled from the growth temperature at the catalyst.

RESULTS AND DISCUSSION

We explore CNT forest growth in a "matrix" of T_s and T_p conditions and employ a complementary set of techniques to precisely determine how these thermal conditions influence the key structural characteristics of CNT forests. While gas-phase reactions occur both in the preheater and in proximity of the substrate, T_p has a dominant effect in causing decomposition and rearrangement of C_2H_4/H_2, whereas the effect of T_s is negligible. To demonstrate this, we analyzed the gas composition flowing out of the reactor during control experiments at three binary ON/OFF combinations where T_s and T_p were set to typical values for this study. Figure 2a shows spectra obtained by online residual gas analysis under these conditions. These measurements reveal that the reactor contains a highly polydisperse atmosphere, and the composition is indifferent to T_s when the gas is thermally treated at T_p before entering the reactor.

Figure 2b displays the partial pressures of the compounds resulting from thermal treatment of C_2H_4/H_2 (0.2/0.8 atm) at approximately T_p = 1020 °C, as collected from the preheater output and analyzed *ex situ* by gas chromatography (GC)−MS and GC−flame ionization detection (FID) by Plata *et al.*[45] These show a multitude of products including various alkanes, alkenes, and alkynes, as well as volatile organic compounds (VOCs) and polycyclic aromatic hydrocarbons (PAHs).[45] Incidentally, the untreated gas mixture (T_s/T_p = 25/25 °C) contains the expected compounds along with naphthalene and acenaphthylene, which are ambient pollutants and derive from typical combustion processes. The variety of thermally generated products, as well as significant variations in relative abundances, demonstrates the complexity of the CVD process and suggests that one or more of the measured species is responsible for enhanced growth rates discussed later. Identifying and related mechanistic understanding of the individual compounds that are responsible for enhanced growth is a focus of ongoing work and exceeds the present scope. However, identifying and quantifying the contents of the polydisperse hydrocarbon atmosphere provides a qualitative framework for interpreting the de-

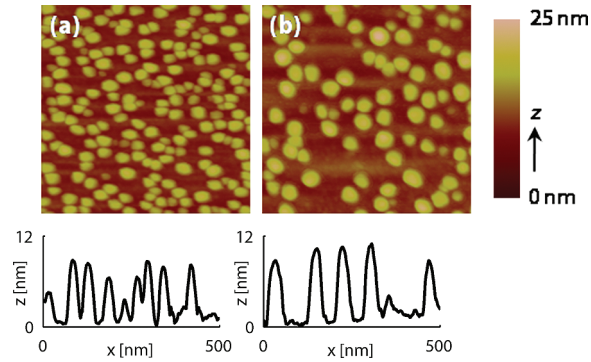

Figure 3. AFM images and corresponding topographical profiles of Fe catalyst on an Al_2O_3 support, annealed in H_2/He for 2 min at (a) T_s = 725 °C and (b) T_s = 875 °C. Shaded bar on the right shows relative topographical height, and each image depicts a 500 nm × 500 nm scan.

coupled roles of T_s and T_p in determining CNT forest characteristics in the present study.

The first step in the CNT growth process is formation of the catalyst particles from the Fe thin film, which is oxidized when exposed to ambient air after deposition and reduced to its metallic state when heated in H_2/He.[38,46] The temperature of catalyst annealing by exposure to a reducing atmosphere before growth, which is equal to T_s during growth, is a principle means of controlling the CNT diameter. Conversely, the activity of the reactant mixture (determined by T_p) has a negligible effect on CNT diameter, which is further discussed later. Upon heating, the Fe film agglomerates rapidly into well-defined nanoparticles, as verified by AFM imaging (Figure 3). In accordance with our AFM results, thin film theory predicts that the mean particle size will increase with higher T_s, so that the free energy of the particles decreases;[47−49] many previous studies have shown correlations between particle size and resultant CNT diameter.[50,51] After initial heating, the particles coarsen slowly and increase in size with continued exposure to H_2, and consequent to conservation of mass, fewer and larger particles are present at longer catalyst annealing times. Upon introduction of C_2H_4, CNTs are thought to be templated by the catalyst nanoparticles, and when a relatively high density of particles are active,[31] CNTs crowd and form a vertically aligned configuration that accommodates continued upward growth as carbon is added at the base.

Mapping the CNT forests by transmission small-angle X-ray scattering (SAXS),[52] and fitting the resultant intensity scans to a mathematical model of a CNT forest as a population of hollow cylinders having a log-normal diameter distribution (Figure 4a and Supporting Information, Figure S1), reveals that the mean CNT diameter is directly related to T_s. A linear relationship is apparent from T_s = 725−875 °C, and CNT diameter values appear to be constant for T_s = 725 °C and below (Figure 4b). TEM imaging verifies SAXS as a precise nondestructive measurement of CNT diameter. Using TEM, we measured mean diameters of 8.0 nm (σ = 1.1) and

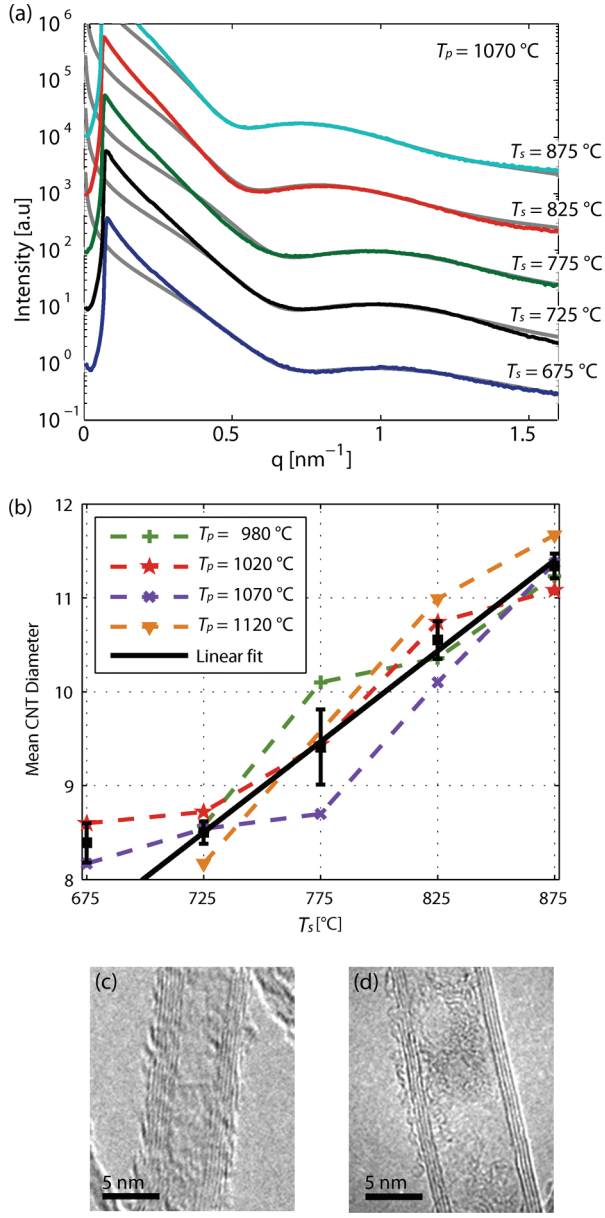

Figure 4. (a) Plots of scattered intensity *versus* scattering vector (gray) taken at the vertical midpoint of forests grown at different T_s values (constant T_p = 1070 °C), and corresponding fits (color) that give the average CNT diameter within the X-ray beampath. (b) Correlation between T_s and diameter is observed over a wide range of T_p values, with a linear relationship persisting between T_s = 725 and 875 °C. The black squares indicate the average diameters for all tested T_p values, and the error bars represent one standard deviation. The TEM images represent CNTs grown at (c) T_s = 675 °C and (d) T_s = 875 °C.

10.5 nm (σ = 2.0) from approximately 60 CNTs grown at each set of thermal conditions T_s/T_p = 675/1020 °C and T_s/T_p = 875/1020 °C, respectively. In comparison, the SAXS data and analysis determine 8.6 nm (σ = 1.7) and 11.1 nm (σ = 2.6) for the respective conditions; these values are within 10% of the TEM data. Further, while the distribution of diameters broadens with increasing T_s, both SAXS and TEM data demonstrate that bimodal populations[53] do not evolve in our system. The explicit dependence of CNT diameter on T_s, which overlaps for a wide range of T_p, demonstrates that the diameter is not strongly influenced by the gas-phase rearrangement of C_2H_4 but rather is driven by the thermal treatment of the catalyst.

Next, while CNT diameter is independent of T_p, the CNT quality is affected strongly by both T_s and T_p. The Raman I_G/I_D peak intensity ratio is an ordinal measure of the amount of sp^2-hybridized carbon *versus* the amount of disordered carbon in the CNT material.[54] Accordingly, Raman spectra (Figure 5) demonstrate that the relative CNT structural quality monotonically increases with T_s. In contrast, I_G/I_D decreases with increasing T_p, suggesting that additional thermal rearrangement of the carbon source leads to lower-quality CNTs. At T_s/T_p = 825/900 °C, I_G/I_D = 2.3, and in comparison, forests grown from the same catalyst composition in a single-zone tube furnace at 775 °C have I_G/I_D = 1.2. A previous study that synthesized CNTs from a C_{60} precursor showed that accumulation of graphite-like deposits on the CNT walls can result in a high I_G/I_D even though the CNT structure itself is poor.[51] However, TEM images (Figure 4c,d) confirm that our CNTs are free of graphitic fragments.

However, Raman spectroscopy cannot quantitatively differentiate between structural defects in CNTs and amorphous carbon deposited on the CNT side walls. Accordingly, thermogravimetric analysis (TGA) provides further insight into the independent roles of gas decomposition and catalyst temperature in determining CNT material quality. Amorphous carbon accumulated on the CNT walls has a lower thermal stability than graphitic CNT carbon, and therefore, the relative amounts of amorphous and graphitic carbon can be related by the relative mass losses at low (~300 °C) and high (~700 °C) temperatures. TGA measurements of our samples (Figure 6) reveal that the proportion of amorphous carbon depends on T_s and T_p, as well as on the growth time, which determines the amount of deposition on the side walls of existing CNTs. CNTs grown by the decoupled method accumulate more amorphous carbon than those grown in a tube furnace; however, the ability to increase the catalyst temperature using the decoupled method gives CNTs with higher structural quality. This is shown by the peak in mass loss rate at about 710 °C for CNTs grown at T_s = 875 °C, as compared to 670 °C for T_s = 675 °C. Increasing T_p and increasing the growth time both increase the amount of amorphous carbon produced on the CNTs, the latter of which is concurrent with other recent reports that correlate amorphous carbon accumulation with prolonged exposure to the growth environment.[55]

Kinetics of CNT forest growth in our process, as measured in real time, show three regions (Figure 7a,b): (1) initial acceleration as the chamber reaches a steady-state reactant composition; (2) a prolonged period of a nearly constant yet gradually decreasing growth rate; and (3) abrupt termination when the growth rate rap-

idly drops to zero.[56] The decay of growth rate with time has previously been attributed to several factors, which may not be mutually exclusive, including diffusion limitation, where activate precursors are restricted from the metal catalysts by the increasing height of the forest;[15,18] decaying catalytic activity as growth proceeds;[12] and/or carbon overcoating or sooting on the surface of the metal catalyst from excessive gas-phase decomposition and rearrangement.[16,24] Reaction-limited kinetics models have also been proposed to describe the growth, but these fail to predict growth deceleration and suggest the rate remains linear indefinitely.[17,18] Growth rate, catalyst lifetime, and terminal forest height all vary with T_s and T_p in our system. However, when the kinetics curves are normalized (Figure 7c), self-similarity is apparent, amid slight deviations in the height measurements due to non-uniformities across the forest surface.

We non-dimensionalize the kinetics as height $h^* = (h)/(h_{term})$ and time $t^* = (t - 0.05 \times t_{life})/(0.95 \times t_{life} - 0.05 \times t_{life})$, where h_{term} is the terminal height of the forest for a given reaction and t_{life} is the catalyst lifetime (defined as the elapsed time between 1 and 99% of h_{term}). Although forests reach various terminal heights at widely varying rates, growth terminates abruptly in all cases. Both diffusion limitation [$h = 0.5\sqrt{(A^2 + 4Bt)} - 0.5A$][19] and catalyst decay [$h = \beta\tau_0(1 - e^{-t/\tau_0})$][12] models fit the steady regime of the observed kinetics, but these models far overestimate the terminal forest height and fail to capture the abrupt termination event.[56] This suggests a sudden mechanism of CNT growth termination, which is not sufficiently described by either diffusion-limited precursor delivery or catalyst decay.

The CNT forest growth rate during the steady period increases monotonically with both T_s and T_p (Figure 8a); however, there is a distinct exchange between steady growth rate and catalyst lifetime (Figure 8c). We define the steady growth rate r_{avg} over the nearly linear portion of each growth curve, extending from 25 to 75% of h_{term}, such that $r_{avg} = (0.75 \times h_{term} - 0.25 \times h_{term})/(0.75 \times t_{life} - 0.25 \times t_{life})$. Growth is fastest at both high T_s and T_p, but the catalyst lifetime is shortest under these conditions. For example, $r_{avg} = 18.5$ μm/s at $T_s/T_p = 875/1120$ °C, but here the terminal height is only 0.5 mm, compared to nearly 4 mm at the more moderate conditions $T_s/T_p = 825/1020$ °C (Figure 8b). Further, the slope of the relationship between r_{avg} and T_p increases with T_s. This is formally quantified by estimating the apparent activation energy E_a of the synthesis reaction using the Arrhenius relation, $\dot{h} \propto k = e^{-E_a/RT_s}$. Here, R is the universal gas constant, and we assume the growth rate $\dot{h}$, which is proportional to the reaction rate k, is approximately equal to r_{avg}. By plotting $\ln(r_{avg})$ *versus* $1/T_s$, we extract E_a from the slope of the linear fits for various T_p values (Figure 8d); our values of E_a monotonically increase with T_p and are comparable to values previously reported for thermal CVD of CNTs.[57,58] The dependence of E_a on T_p suggests that the cumulative process of gas decomposition and rearrangement is a rate-determining step in CNT forest growth. Finally, the synergy between T_s and T_p appears to only be activated at $T_s = 775$ °C and above. This indicates a threshold beyond which interaction between the population of thermally generated hydrocarbon precursors and catalyst conditions nonlinearly enhances the rate of CNT growth from Fe on Al_2O_3.

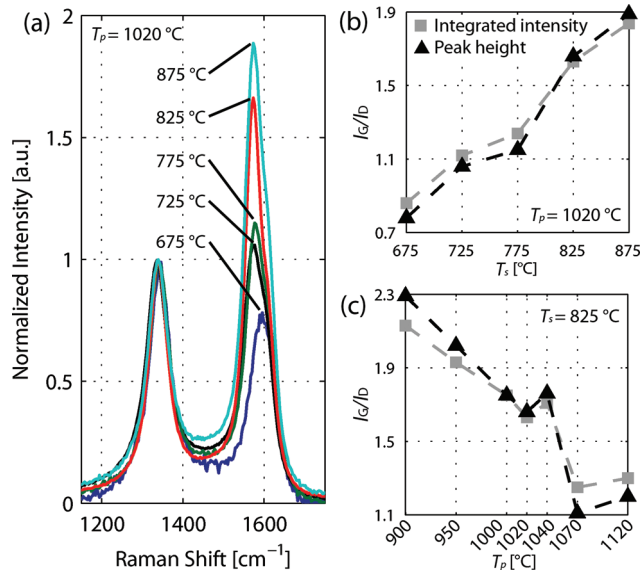

Figure 5. (a) Averaged, normalized Raman spectra acquired for five CNT forests grown at different T_s (constant T_p = 1020 °C). (b) Data from (a) analyzed and plotted *versus* T_s show that I_G/I_D monotonically increases with T_s. (c) Dependence of I_G/I_D on T_p with constant T_s (825 °C) also illustrates that CNT material quality degrades as T_p increases. I_G/I_D is calculated by both considering the peak heights (black triangles) and integrating the intensity curves (gray squares).

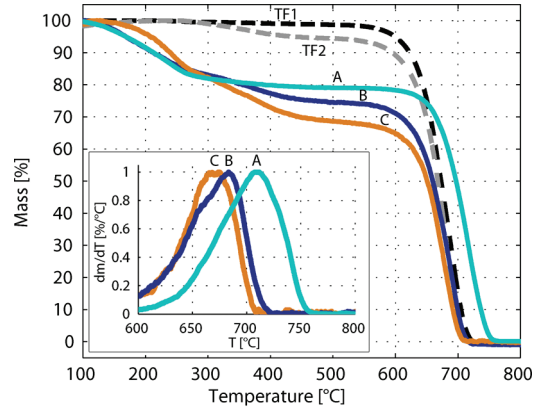

	A	B	C	TF1	TF2
T_s	875 °C	675 °C	825 °C	775 °C*	775 °C*
T_p	1020 °C	1020 °C	1120 °C		
t_{growth}	8 min.	20 min.	1 min.	20 min.	60 min.

*Single-zone setpoint

Figure 6. TGA of CNT forests synthesized under various conditions and reactors. The curves show mass loss as a function of oxidation temperature, while the inset depicts normalized curves of the rate of mass loss. Synthesis conditions are detailed in the table below the plot.

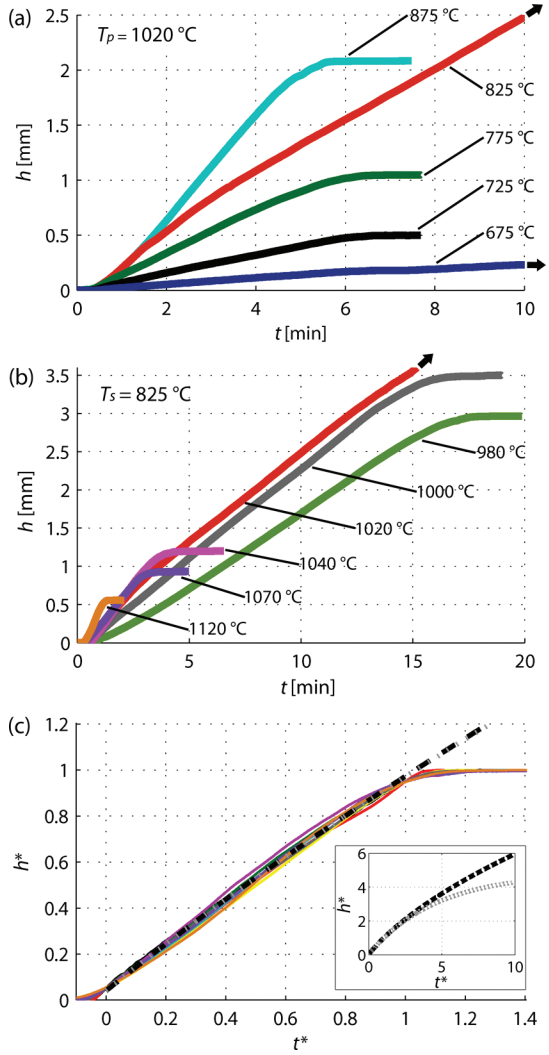

Figure 7. (a) Height *versus* time curves for various T_s values (constant T_p = 1020 °C). The T_s = 825 °C curve terminates beyond 3.6 mm where the laser signal is lost, and the T_s = 675 °C curve reaches a terminal height of 400 μm after 20 min. (b) Height *versus* time curves for various T_p values (constant T_s = 825 °C), and the T_p = 1020 °C curve terminates beyond 3.6 mm. (c) Normalized kinetics from (a) and (b) with quadratic decay and β decay fits of this self-similar curve (fits shown in black and gray dashed curves). The inset emphasizes that these models significantly overestimate the terminal CNT length.

The catalyst lifetime is primarily determined by the extent of thermal treatment of the feedstock gas (Figure 8c), that is, the preheater temperature T_p. Our further gas analysis, which will be reported separately, shows that the relative abundance of certain hydrocarbon species increases by orders of magnitude with marginal increases in T_p.[45] While we show that varying T_p can enhance the growth process (*e.g.*, increased r_{avg} or h_{term}), there is a corresponding drop in catalyst lifetime with higher T_p for all values of T_s. Further, while lowering T_p generally prolongs catalytic activity, there is a limit to this effect. That is, catalyst lifetime increases nonlinearly as T_p decreases and reaches a maximum at T_p = 950 °C, but below this temperature, it drops severely again, leading to relatively ineffective growth. This sharp transition suggests that some constituent parts of the decomposed gas mixture may be absent at low T_p (<950 °C), whereas at high T_p, select compounds may present considerable obstacles to one or more aspects of the growth process (*e.g.*, carbon deposition on the catalyst). Decaying trends in kinetic parameters have been previously discussed,[24] and while we show a persistent increase in growth rate, we do observe decays in lifetime and height at high temperatures.

TABLE 1. Tunable CNT Forest Characteristics *via* Independent Control of Thermal Conditions

	control parameters	
characteristics	increase T_s constant T_p	increase T_p constant T_s
CNT diameter	↑	–
I_G/I_D	↑	↓
growth rate	↑	↑
terminal height	↑	first ↑ then ↓
catalyst lifetime	–	↓[a]

[a]From T_p = 950 °C.

Overall, to attain efficient growth of tall CNT forests, we must balance the reaction rate and catalyst lifetime, which is practically achieved by moderate T_p values. Thermal control at the catalyst is also critical, as forest height increases with T_s (Figure 8b); however, optimum heights are realized at T_s = 825 °C, not 875 °C, which could be the result of compromised catalyst performance due to excessive heating. Table 1 summarizes the dependence of CNT forest characteristics on the temperature of the catalyst (T_s) and on the thermal decomposition temperature (T_p) of the reactant mixture. Independent tuning of characteristics can be achieved in many cases with the appropriate combination of thermal conditions since diameter and lifetime are governed by only one thermal parameter.

CONCLUSION

Decoupling thermal treatment of the precursor and catalyst enables new understanding of the mechanisms determining diameter, quality, and kinetics of CNT growth in a vertically aligned forest configuration. Increasing both temperatures (T_s and T_p) enhances the growth rate, yet terminal forest height, catalyst lifetime, and CNT quality suffer from excessive gas decomposition and/or catalyst deactivation at high temperature conditions. This suggests the existence of competing pathways between graphitic and amorphous carbon deposited during synthesis and highlights a deficiency of CVD processes in which these thermal control parameters are coupled. To this extent, we demonstrate the generation a broad population of PAHs and VOCs in the CVD atmosphere, suggesting a role of select carbon species in either enhancing or inhibiting efficient

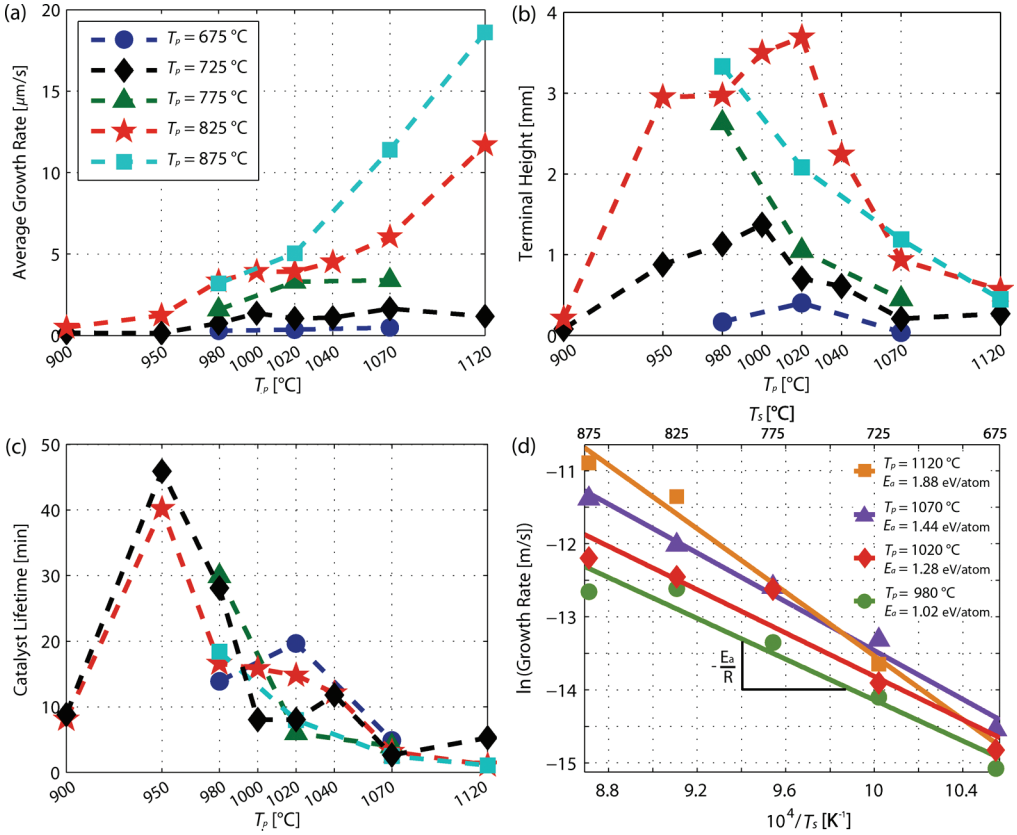

Figure 8. Kinetics trends for CNT forest growth under various temperature conditions: (a) average steady growth rate, (b) terminal forest height, (c) lifetime of the catalyst, and (d) Arrhenius plots with associated apparent activation energies (E_a).

and/or prolonged forest growth. The precise mechanism of CNT forest growth termination remains unclear; however, it is reasonable to conclude that the large population of hydrocarbons resulting from thermal decomposition introduces constituent species that promote efficient forest growth, while others drive the catalyst into a state unfavorable for continuous deposition of graphitic carbon. By exploiting the interplay between T_s and T_p, we enhance the resultant I_G/I_D to generate as-grown, high-quality forests without implementing post-treatment purification steps,[59−63] which are often energy and time consumptive as well as destructive to the aligned structure of a forest. Self-similarity of CNT forest growth kinetics suggests the existence of a universal and sudden termination mechanism that may limit indefinite growth of CNTs. Further, our decoupled processing method, supported by closed-loop automated control of the growth reactor, enables rapid mapping of a broad parameter space. Extension of this study to other catalyst film thicknesses (*e.g.*, thinner catalyst films, which would be expected to give smaller diameter CNTs) and compositions could help establish application-oriented structure−property maps for CNTs.

METHODS

We explored a "matrix" of T_s and T_p conditions, namely, T_s = {675, 725, 775, 825, 875 °C} and T_p = {900, 950, 980, 1000, 1020, 1040, 1070, 1120 °C}. The growth substrate was 1/10 nm Fe/Al_2O_3, deposited by electron beam evaporation on a (100) silicon wafer coated with 100 nm thermally grown SiO_2.[23] All experiments were performed on 1 cm^2 catalyst substrates taken from the same Si wafer. For each experiment, the chamber was first flushed with He for 10 min, then flushed with 310/300 sccm H_2/He for 2 min. Then, the substrate was rapidly heated to T_s for 2 min before the atmosphere was adjusted to 120/310/180 sccm C_2H_4/H_2/He and held throughout the duration of growth. The gases were always passed through the heated pipe (4 mm i.d.), wrapped with a resistively heated coil (~70 mm long heated zone). Before the substrate was heated, the pipe was ramped to the desired set point T_p, as measured by a thermocouple placed halfway along the length of the coil. Reactions were performed at atmospheric pressure. Online quadrupole mass spectrometer residual gas analyzer (Pfeiffer OmniStar GSD 301) was plumbed into the exhaust port of the reaction chamber with a stainless steel capillary.

A dedicated LabVIEW interface was built to monitor and control the process variables: (1) T_s was measured using an infrared sensor (Exergen 2ACF-K-HIE) and controlled using a high-speed PID controller (RKC Instruments, model HA400, 40 Hz sampling rate); (2) T_p was measured using a K-type thermocouple and controlled using a PID controller (Omega CNi-series); (3) forest height was dynamically measured using a laser displacement sensor (Keyence LK-G152); and (4) gas flow rates were measured and controlled using digital mass flow controllers (Aalborg GFC 17, response time = 2 s). Experiments were fully automated by preloading programmed recipes, thus increasing throughput and reducing experimental error. The sampling rate, 8 samples/s, is set by the loop execution time, which depends on the speed of the processor and the complexity of the data logging.

AFM imaging was performed in tapping mode (MultiMode AFM, Nanoscope IIIa controller), and results were analyzed using WSxM 3.0 Beta 12.1.[64] Samples were prepared by heating the substrate in 310/300 sccm H_2/He for 2 min, and then rapidly cooling the substrate in H_2/He without exposure to C_2H_4.

CNT diameters were measured nondestructively by transmission SAXS, which was performed at the X27C beamline at the National Synchrotron Light Source (NSLS) at Brookhaven National Laboratory. X-ray wavelength was 0.1371 nm with a spot size of approximately 0.3 mm in diameter. As described previously,[52] the integrated $I-q$ taken from each SAXS image was fit using a form factor relationship for a log-normal distribution of hollow cylinders (see Supporting Information). This provides a nondestructive measurement of the mean CNT diameter and polydispersity within the X-ray beampath through each forest and agrees with diameter measurements based on TEM images for large numbers of individual CNTs. SEM (Philips XL30 FEG) and TEM (JEOL 3011 HREM) imaging were performed at the University of Michigan Electron Microbeam Analysis Laboratory (EMAL). TEM images were processed and analyzed with Infinity Analyze Version 4.5.

CNT structural quality was evaluated by Raman spectroscopy (Dimension P2, Lambda Solutions, $\lambda = 533$ nm), and several spectra per sample were acquired along the midpoint of the forest side wall and averaged. For thermogravimetric analysis (TGA), forests were delaminated from the growth substrate and heated from room temperature to 1000 °C at 10 °C/min in 20 sccm air flow (Perkin-Elmer Pyris 1 TGA). From Table 1, samples A, B, and C were synthesized by our decoupled method with specified T_s and T_p, while samples TF1 and TF2 were synthesized in a commercial single-zone tube furnace, where the thermal conditions for gas decomposition were defined by the temperature profile along the heated path preceding the growth substrate.

The PAH, alkene, and alkane quantity of reactant gas mixtures were determined as described by Plata *et al.*[45] Briefly, polyurethane foam filters were used to concentrate PAHs over the entire course of the synthetic reaction. These filters were then extracted with organic solvents (dichloromethane and methanol), concentrated by rotary evaporation, and analyzed by gas chromatography−mass spectrometry (GC−MS). Gases that survived transit through the foam filter were collected in a stainless steel canister, cryogenically concentrated, and subsequently analyzed by GC−MS (hydrocarbon identification), GC−flame ionization detection (hydrocarbon identification and quantification), and GC−thermal conductivity detection (helium and hydrogen quantification).

Acknowledgment. This work was funded by the University of Michigan Department of Mechanical Engineering and College of Engineering, and the National Science Foundation (CMMI-0800213). E.R.M. and S.T. are grateful for University of Michigan Mechanical Engineering Departmental Fellowships. D.L.P. acknowledges support by the National Science Foundation Graduate Research Fellowship Program, WHOI's Ocean Ventures Fund, the Chesonis family through the MIT Earth System Initiative, and the Martin Family Society of Graduate Fellows for Sustainability. E.A.V. is grateful to the Institute for Soldier Nanotechnologies at MIT, funded by the U.S. Army Research Office (DAAD-19-02-D0002). X-ray scattering was performed at the National Synchrotron Light Source, Brookhaven National Laboratory, which is supported by the U.S. Department of Energy Office of Basic Energy Sciences (DE-AC02-98CH10886). SEM and TEM were performed at the University of Michigan Electron Microbeam Analysis Laboratory (EMAL). We thank Kyle Yazzie, Jeremy Ng, Namiko Yamamoto, Kevin Critchley, and Sudhanshu Srivastava for assistance with X-ray scattering, SAXS data processing, catalyst preparation, AFM, and TGA, respectively. We also thank Nicholas Kotov for graciously sharing his AFM and TGA facilities, as well as Philip Gschwend, Christopher Reddy, and Jeffrey Seewald for providing PAH and VOC analytical instrumentation, and for enlightening discussions on these topics.

Supporting Information Available: Details our method of fitting a model to the SAXS data; sample scattering intensity image and an additional set of $I-q$ plots with curve fits; CNT diameter statistics measured by TEM. This material is available free of charge *via* the Internet at http://pubs.acs.org.

REFERENCES AND NOTES

1. Kong, J.; Soh, H.; Cassell, A.; Quate, C.; Dai, H. Synthesis of Individual Single-Walled Carbon Nanotubes on Patterned Silicon Wafers. *Nature* **1998**, *395*, 878–881.
2. Fan, S. S.; Chapline, M. G.; Franklin, N. R.; Tombler, T. W.; Cassell, A. M.; Dai, H. J. Self-Oriented Regular Arrays of Carbon Nanotubes and Their Field Emission Properties. *Science* **1999**, *283*, 512–514.
3. Baughman, R. H.; Zakhidov, A. A.; de Heer, W. A. Carbon Nanotubes—The Route toward Applications. *Science* **2002**, *297*, 787–792.
4. Endo, M.; Hayashi, T.; Kim, Y.; Terrones, M.; Dresselhaus, M. Applications of Carbon Nanotubes in the Twenty-First Century. *Philos. Trans. R. Soc. London, Ser. A* **2004**, *362*, 2223–2238.
5. García, E. J.; Wardle, B. L.; Hart, A. J. Joining Prepreg Composite Interfaces with Aligned Carbon Nanotubes. *Compos. Part A* **2008**, *39*, 1065–1070.
6. Tong, T.; Zhao, Y.; Delzeit, L.; Kashani, A.; Meyyappan, M.; Majumdar, A. Dense, Vertically Aligned Multiwalled Carbon Nanotube Arrays as Thermal Interface Materials. *IEEE Trans. Compon. Technol.* **2007**, *30*, 92–100.
7. Choi, W.; Chung, D.; Kang, J.; Kim, H.; Jin, Y.; Han, I.; Lee, Y.; Jung, J.; Lee, N.; Park, G.; Kim, J. Fully Sealed, High-Brightness Carbon-Nanotube Field-Emission Display. *Appl. Phys. Lett.* **1999**, *75*, 3129–3131.
8. Holt, J.; Park, H.; Wang, Y.; Stadermann, M.; Artyukhin, A.; Grigoropoulos, C.; Noy, A.; Bakajin, O. Fast Mass Transport Through Sub-2-Nanometer Carbon Nanotubes. *Science* **2006**, *312*, 1034–1037.
9. Hinds, B.; Chopra, N.; Rantell, T.; Andrews, R.; Gavalas, V.; Bachas, L. Aligned Multiwalled Carbon Nanotube Membranes. *Science* **2004**, *303*, 62–65.
10. Dell'Acqua-Bellavitis, L.; Ballard, J.; Ajayan, P.; Siegel, R. Kinetics for the Synthesis Reaction of Aligned Carbon Nanotubes: A Study Based on *In Situ* Diffractography. *Nano Lett.* **2004**, *4*, 1613–1620.
11. Einarsson, E.; Murakami, Y.; Kadowaki, M.; Maruyama, S. Growth Dynamics of Vertically Aligned Single-Walled Carbon Nanotubes from *In Situ* Measurements. *Carbon* **2008**, *46*, 923–930.
12. Futaba, D.; Hata, K.; Yamada, T.; Mizuno, K.; Yumura, M.; Iijima, S. Kinetics of Water-Assisted Single-Walled Carbon Nanotube Synthesis Revealed by a Time-Evolution Analysis. *Phys. Rev. Lett.* **2005**, *95*, 056104.
13. Han, J.; Graff, R.; Welch, B.; Marsh, C.; Franks, R.; Strano, M. A Mechanochemical Model of Growth Termination in Vertical Carbon Nanotube Forests. *ACS Nano* **2008**, *2*, 53–60.
14. Liu, K.; Jiang, K.; Feng, C.; Chen, Z.; Fan, S. A Growth Mark Method for Studying Growth Mechanism of Carbon Nanotube Arrays. *Carbon* **2005**, *43*, 2850–2856.
15. Louchev, O.; Laude, T.; Sato, Y.; Kanda, H. Diffusion-Controlled Kinetics of Carbon Nanotube Forest Growth by Chemical Vapor Deposition. *J. Chem. Phys.* **2003**, *118*, 7622–7634.
16. Puretzky, A.; Geohegan, D.; Jesse, S.; Ivanov, I.; Eres, G. In Situ Measurements and Modeling of Carbon Nanotube Array Growth Kinetics During Chemical Vapor Deposition. *Appl. Phys. A* **2005**, *81*, 223–240.
17. Xiang, R.; Yang, Z.; Zhang, Q.; Luo, G.; Qian, W.; Wei, F.; Kadowaki, M.; Einarsson, E.; Maruyama, S. Growth Deceleration of Vertically Aligned Carbon Nanotube Arrays: Catalyst Deactivation or Feedstock Diffusion Controlled. *J. Phys. Chem. C* **2008**, *112*, 4892–4896.
18. Zhu, L.; Xu, J.; Xiao, F.; Jiang, H.; Hess, D.; Wong, C. The Growth of Carbon Nanotube Stacks in the Kinetics-Controlled Regime. *Carbon* **2007**, *45*, 344–348.
19. Zhu, L.; Hess, D.; Wong, C. Monitoring Carbon Nanotube Growth by Formation of Nanotube Stacks and

Investigation of the Diffusion-Controlled Kinetics. *J. Phys. Chem. B* **2006**, *110*, 5445–5449.
20. Zhang, G. Y.; Mann, D.; Zhang, L.; Javey, A.; Li, Y. M.; Yenilmez, E.; Wang, Q.; McVittie, J. P.; Nishi, Y.; Gibbons, J.; Dai, H. J. Ultra-High-Yield Growth of Vertical Single-Walled Carbon Nanotubes: Hidden Roles of Hydrogen and Oxygen. *Proc. Natl. Acad. Sci. U.S.A.* **2005**, *102*, 16141–16145.
21. Hata, K.; Futaba, D. N.; Mizuno, K.; Namai, T.; Yumura, M.; Iijima, S. Water-Assisted Highly Efficient Synthesis of Impurity-Free Single-Waited Carbon Nanotubes. *Science* **2004**, *306*, 1362–1364.
22. Delzeit, L.; Nguyen, C. V.; Chen, B.; Stevens, R.; Cassell, A.; Han, J.; Meyyappan, M. Multiwalled Carbon Nanotubes by Chemical Vapor Deposition Using Multilayered Metal Catalysts. *J. Phys. Chem. B* **2002**, *106*, 5629–5635.
23. Hart, A.; Slocum, A. Rapid Growth and Flow-Mediated Nucleation of Millimeter-Scale Aligned Carbon Nanotube Structures from a Thin-Film Catalyst. *J. Phys. Chem. B* **2006**, *110*, 8250–8257.
24. Wood, R. F.; Pannala, S.; Wells, J. C.; Puretzky, A. A.; Geohegan, D. B. Simple Model of the Interrelation between Single- and Multiwall Carbon Nanotube Growth Rates for the CVD Process. *Phys. Rev. B* **2007**, *75*, 8.
25. Lacava, A. I.; Bernardo, C. A.; Trimm, D. L. Studies of Deactivation of Metals by Carbon Deposition. *Carbon* **1982**, *20*, 219–223.
26. Kaatz, F.; Siegal, M.; Overmyer, D.; Provencio, P.; Jackson, J. Diameter Control and Emission Properties of Carbon Nanotubes Grown Using Chemical Vapor Deposition. *Mater. Sci. Eng. C* **2003**, *23*, 141–144.
27. Yuan, Z.; Huang, H.; Liu, L.; Fan, S. Controlled Growth of Carbon Nanotubes in Diameter and Shape Using Template-Synthesis Method. *Chem. Phys. Lett.* **2001**, *345*, 39–43.
28. Fu, Q.; Huang, S.; Liu, J. Chemical Vapor Depositions of Single-Walled Carbon Nanotubes Catalyzed by Uniform Fe_2O_3 Nanoclusters Synthesized Using Diblock Copolymer Micelles. *J. Phys. Chem. B* **2004**, *108*, 6124–6129.
29. Lu, J.; Kopley, T.; Moll, N.; Roitman, D.; Chamberlin, D.; Fu, Q.; Liu, J.; Russell, T.; Rider, D.; Manners, I.; Winnik, M. High-Quality Single-Walled Carbon Nanotubes with Small Diameter, Controlled Density, and Ordered Locations Using a Polyferrocenylsilane Block Copolymer Catalyst Precursor. *Chem. Mater.* **2005**, *17*, 2227–2231.
30. Bennett, R. D.; Xiong, G. Y.; Ren, Z. F.; Cohen, R. E. Using Block Copolymer Micellar Thin Films as Templates for the Production of Catalysts for Carbon Nanotube Growth. *Chem. Mater.* **2004**, *16*, 5589–5595.
31. Bennett, R. D.; Hart, A. J.; Cohen, R. E. Controlling the Morphology of Carbon Nanotube Films by Varying the Areal Density of Catalyst Nanoclusters Using Block-Copolymer Micellar Thin Films. *Adv. Mater.* **2006**, *18*, 2274–2279.
32. Ishida, M.; Hongo, H.; Nihey, F.; Ochiai, Y. Diameter-Controlled Carbon Nanotubes Grown from Lithographically Defined Nanoparticles. *Jpn. J. Appl. Phys.* **2004**, *43*, L1356–L1358.
33. Wei, Y.; Eres, G.; Merkulov, V.; Lowndes, D. Effect of Catalyst Film Thickness on Carbon Nanotube Growth by Selective Area Chemical Vapor Deposition. *Appl. Phys. Lett.* **2001**, *78*, 1394–1396.
34. Zhao, B.; Futaba, D. N.; Yasuda, S.; Akoshima, M.; Yamada, T.; Hata, K. Exploring Advantages of Diverse Carbon Nanotube Forests with Tailored Structures Synthesized by Supergrowth from Engineered Catalysts. *ACS Nano* **2009**, *3*, 108–114.
35. Chhowalla, M.; Teo, K.; Ducati, C.; Rupesinghe, N.; Amaratunga, G.; Ferrari, A.; Roy, D.; Robertson, J.; Milne, W. Growth Process Conditions of Vertically Aligned Carbon Nanotubes Using Plasma Enhanced Chemical Vapor Deposition. *J. Appl. Phys.* **2001**, *90*, 5308–5317.
36. Ho, G.; Wee, A.; Lin, J.; Tjiu, W. Synthesis of Well-Aligned Multiwalled Carbon Nanotubes on Ni Catalyst Using Radio Frequency Plasma-Enhanced Chemical Vapor Deposition. *Thin Solid Films* **2001**, *388*, 73–77.
37. Lee, C.; Lyu, S.; Cho, Y.; Lee, J.; Cho, K. Diameter-Controlled Growth of Carbon Nanotubes Using Thermal Chemical Vapor Deposition. *Chem. Phys. Lett.* **2001**, *341*, 245–249.
38. Nessim, G. D.; Hart, A. J.; Kim, J. S.; Acquaviva, D.; Oh, J.; Morgan, C. D.; Seita, M.; Leib, J. S.; Thompson, C. V. Tuning of Vertically-Aligned Carbon Nanotube Diameter and Areal Density Through Catalyst Pre-Treatment. *Nano Lett.* **2008**, *8*, 3587–3593.
39. Choi, Y.; Shin, Y.; Lee, Y.; Lee, B.; Park, G.; Choi, W.; Lee, N.; Kim, J. Controlling the Diameter, Growth Rate, and Density of Vertically Aligned Carbon Nanotubes Synthesized by Microwave Plasma-Enhanced Chemical Vapor Deposition. *Appl. Phys. Lett.* **2000**, *76*, 2367–2369.
40. van Laake, L.; Hart, A. J.; Slocum, A. H. Suspended Heated Silicon Platform for Rapid Thermal Control of Surface Reactions with Application to Carbon Nanotube Synthesis. *Rev. Sci. Instrum.* **2007**, *78*, 083901.
41. Hart, A. J.; van Laake, L.; Slocum, A. H. Desktop Growth of Carbon-Nanotube Monoliths with *In Situ* Optical Imaging. *Small* **2007**, *3*, 772–777.
42. Chaisitsak, S.; Yamada, A.; Konagai, M. Hot Filament Enhanced CVD Synthesis of Carbon Nanotubes by Using a Carbon Filament. *Diamond Relat. Mater.* **2004**, *13*, 438–444.
43. Ishikawa, Y.; Jinbo, H. Synthesis of Multiwalled Carbon Nanotubes at Temperatures Below 300 Degrees C by Hot-Filament Assisted Chemical Vapor Deposition. *Jpn. J. Appl. Phys.* **2005**, *44*, L394–L397.
44. Xu, Y. Q.; Flor, E.; Kim, M. J.; Hamadani, B.; Schmidt, H.; Smalley, R. E.; Hauge, R. H. Vertical Array Growth of Small Diameter Single-Walled Carbon Nanotubes. *J. Am. Chem. Soc.* **2006**, *128*, 6560–6561.
45. Plata, D. L.; Hart, A. J.; Reddy, C. M.; Gschwend, P. M. Early Evaluation of Environmental Impacts of Carbon Nanotube Synthesis by Catalytic Chemical Vapor Deposition Submitted for publication.
46. Hofmann, S.; Blume, R.; Wirth, C. T.; Cantoro, M.; Sharma, R.; Ducati, C.; Havecker, M.; Zafeiratos, S.; Schnoerch, P.; Oestereich, A.; Teschner, D.; Albrecht, M.; Knop-Gericke, A.; Schlogl, R.; Robertson, J. State of Transition Metal Catalysts During Carbon Nanotube Growth. *J. Phys. Chem. C* **2009**, *113*, 1648–1656.
47. Ardell, A. J. Experimental Confirmation of the Lifshitz-Wagner Theory of Particle Coarsening. Proceedings of the Mechanism of Phase Transformations in Crystalline Solids, Manchester, UK, 1968.
48. Atwater, H. A.; Yang, C. M. Island Growth and Coarsening in Thin-Films—Conservative and Nonconservative Systems. *J. Appl. Phys.* **1990**, *67*, 6202–6213.
49. Thompson, C. V. Coarsening of Particles on a Planar Substrate−Interface Energy Anisotropy and Application to Grain-Growth in Thin Films. *Acta Metall. Sin.* **1988**, *36*, 2929–2934.
50. Kukovitsky, E. F.; L'Vov, S. G.; Sainov, N. A.; Shustov, V. A.; Chernozatonskii, L. A. Correlation between Metal Catalyst Particle Size and Carbon Nanotube Growth. *Chem. Phys. Lett.* **2002**, *355*, 497–503.
51. Nerushev, O. A.; Dittmar, S.; Morjan, R. E.; Rohmund, F.; Campbell, E. E. B. Particle Size Dependence and Model for Iron-Catalyzed Growth of Carbon Nanotubes by Thermal Chemical Vapor Deposition. *J. Appl. Phys.* **2003**, *93*, 4185–4190.
52. Wang, B.; Bennett, R.; Verploegen, E.; Hart, A.; Cohen, R. Quantitative Characterization of the Morphology of Multiwall Carbon Nanotube Films by Small-Angle X-ray Scattering. *J. Chem. Phys. C* **2007**, *111*, 5859–5865.
53. Nerushev, O. A.; Morjan, R. E.; Ostrovskii, D. I.; Sveningsson, M.; Jönsson, M.; Rohmund, F.; Campbell, E. E. B. The Temperature Dependence of Fe-Catalysed Growth of Carbon Nanotubes on Silicon Substrates. Proceedings of the Tsukuba Symposium on Carbon Nanotube in Commemoration of the 10th Anniversary of Its Discovery2002; Vol. 323, pp 51−59.
54. Dresselhaus, M. S.; Dresselhaus, G.; Saito, R.; Jorio, A.

Raman Spectroscopy of Carbon Nanotubes. *Phys. Rep.* **2005**, *409*, 47–99.
55. Yasuda, S.; Hiraoka, T.; Futaba, D. N.; Yamada, T.; Yumura, M.; Hata, K. Existence and Kinetics of Graphitic Carbonaceous Impurities in Carbon Nanotube Forests to Assess the Absolute Purity. *Nano Lett.* **2009**, *9*, 769–773.
56. Meshot, E.; Hart, A. Abrupt Self-Termination of Vertically Aligned Carbon Nanotube Growth. *Appl. Phys. Lett.* **2008**, *92*, 113107.
57. Hofmann, S.; Kleinsorge, B.; Ducati, C.; Ferrari, A. C.; Robertson, J. Low-Temperature Plasma Enhanced Chemical Vapour Deposition of Carbon Nanotubes. Proceedings of the 14th European Conference on Diamond, Diamond-Like Materials, Carbon Nanotubes, Nitrides and Silicon Carbide2004; Vol. 13, pp 1171−1176.
58. Hofmann, S.; Csanyi, G.; Ferrari, A.; Payne, M.; Robertson, J. Surface Diffusion: The Low Activation Energy Path for Nanotube Growth. *Phys. Rev. Lett.* **2005**, *95*, 036101.
59. Tohji, K.; Takahashi, H.; Shinoda, Y.; Shimizu, N.; Jeyadevan, B.; Matsuoka, I.; Saito, Y.; Kasuya, A.; Ito, S.; Nishina, Y. Purification Procedure for Single-Walled Nanotubes. *J. Phys. Chem. B* **1997**, *101*, 1974–1978.
60. Rinzler, A. G.; Liu, J.; Dai, H.; Nikolaev, P.; Huffman, C. B.; Rodríguez-Macías, F. J.; Boul, P. J.; Lu, A. H.; Heymann, D.; Colbert, D. T.; Lee, R. S.; Fischer, J. E.; Rao, A. M.; Eklund, P. C.; Smalley, R. E. Large-Scale Purification of Single-Wall Carbon Nanotubes: Process, Product, and Characterization. *Appl. Phys. A* **1998**, *67*, 29–37.
61. Shelimov, K. B.; Esenaliev, R. O.; Rinzler, A. G.; Huffman, C. B.; Smalley, R. E. Purification of Single-Wall Carbon Nanotubes by Ultrasonically Assisted Filtration. *Chem. Phys. Lett.* **1998**, *282*, 429–434.
62. Zimmerman, J. L.; Bradley, R. K.; Huffman, C. B.; Hauge, R. H.; Margrave, J. L. Gas-Phase Purification of Single-Wall Carbon Nanotubes. *Chem. Mater.* **2000**, *12*, 1361–1366.
63. Yamada, T.; Namai, T.; Hata, K.; Futaba, D. N.; Mizuno, K.; Fan, J.; Yudasaka, M.; Yumura, M.; Iijima, S. Size-Selective Growth of Double-Walled Carbon Nanotube Forests from Engineered Iron Catalysts. *Nat. Nanotechnol.* **2006**, *1*, 131–136.
64. Horcas, I.; Fernandez, R.; Gomez-Rodriguez, J.; Colchero, J.; Gomez-Herrero, J.; Baro, A. WSXM: A Software for Scanning Probe Microscopy and a Tool for Nanotechnology. *Rev. Sci. Instrum.* **2007**, *78*, 013705.